JOURNAL OF CATALYSIS 63, 265–269 (1980)

Contrast Effects in the Transmission Electron Microscopy of Supported Crystalline Catalyst Particles

Electron microscopy is increasingly used as a technique for the study of supported catalyst particles, providing information about shapes (*1–3*), sizes (*4–6*), internal structure (*3, 7, 8*), and disposition (*4, 5, 9, 10*) on the support (termed "substrate" in this article). Image contrast effects, however, are not always sufficiently appreciated in the field and can greatly complicate interpretation of the results (*11*). Here we draw attention first to amplitude contrast effects which may invalidate recent electron microscope evidence for the thin raftlike structures believed to be present in some catalysts (*12, 13*) and, second, to phase contrast effects, significant in high-resolution studies of small particles whose images can often in consequence be confused with substrate structure.

Amplitude Contrast

Amplitude contrast arises because electrons are scattered outside the objective aperture and are lost to the usual bright-field image which consequently appears dark in the scattering region (*14*). In the case of small crystals, the main scattering mechanism is Bragg reflection which depends strongly on orientation and generally makes amplitude or diffraction contrast the dominating effect for particle sizes above about 3 nm.

An example of the amplitude contrast effects typically observed in supported catalyst particles is shown in Fig. 1. The specimen is of 5 wt% Pd-on-charcoal which has been sintered in hydrogen at 800°C and was prepared for electron microscopy by embedding in resin and slicing with an ultramicrotome to a thickness of ~40 nm. A large variation in contrast is observable between particles of similar widths, such as A and B in Fig. 1a. The crystallites displaying the stronger contrast, such as A, are Bragg reflecting (diffraction contrast), whereas crystallites such as B are not in the correct orientation for Bragg reflection and show weaker amplitude contrast mainly due to diffuse scattering.

For a crystal of thickness t, in the exact Bragg condition, the simple dynamical expression for the coherent diffracted intensity (*14*) is

$$I_{\text{Bragg}} = \sin^2(\pi t/\xi_{hkl}), \qquad (1)$$

where ξ_{hkl} is the extinction distance for the hkl planes involved. (For Pd, $\xi_{111} = 20.6$ nm and $\xi_{200} = 23.6$ nm at 100 keV.) Clearly the Bragg scattered intensity can be comparable with unity leading to very strong contrast and can also oscillate as a function of local thickness t, giving rise to thickness fringes. The bright ring on particle A corresponds to a thickness fringe for $t \simeq \xi_{111}$ and its position indicates that the particle is quasi-spherical.

In the absence of Bragg reflections the residual amplitude contrast is mainly due to incoherent diffuse scattering where (*14*) the scattered intensity is given by

$$I_{\text{diffuse}} = 1 - \exp\left(-\frac{2\pi t}{\xi_0'}\right) \simeq \frac{2\pi t}{\xi_0'}. \qquad (2)$$

For Pd, the value of $\xi_0'/2\pi$ is about 38 nm so that for particles of the size shown in Fig. 1 it is a relatively weak amplitude contrast mechanism as indicated by particle B through which the substrate structure can be seen.

0021-9517/80/050265-05$02.00/0

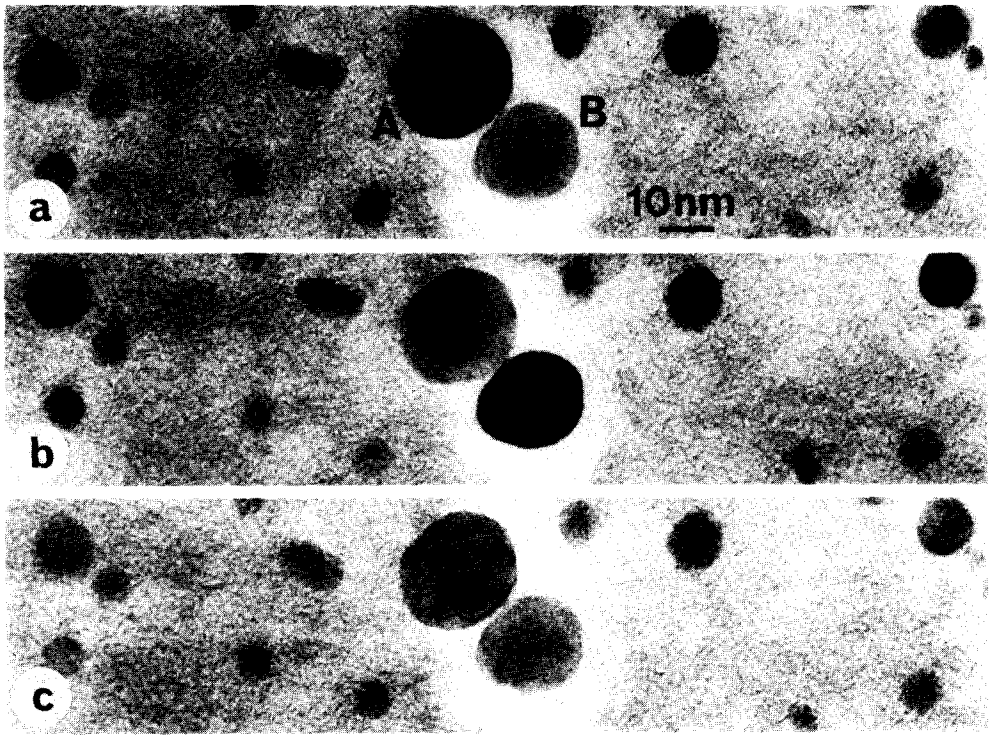

FIG. 1. Diffraction contrast in supported crystalline Pd particles (5 wt% Pd-on-charcoal). (a) 0° tilt; (b) 1.5° tilt; (c) 3° tilt.

In Fig. 1b, the specimen has been tilted through 1.5° thereby altering the diffraction conditions of some of the crystallites. Particle A is now no longer Bragg reflecting and displays the weaker contrast due to diffuse scattering, whereas B is now diffracting in the 111 condition. The bright thickness fringe on B occurs near its center, verifying that it is also roughly spherical in shape. Further specimen tilt (Fig. 1c) again alters the contrast so that neither A nor B is diffracting, so they both appear transparent and thin.

Clearly it is essential to carry out tilting experiments to check for the occurrence of diffraction contrast effects before interpreting the contrast too literally in terms of an absorption effect. It seems likely that the contrast effects interpreted by Prestridge *et al.* (*12*) as due to a mixture of quasi-spherical particles and thin raftlike particles were in fact due to diffraction contrast similar to that described here and previously pointed out in catalysts by Flynn *et al.* (*11*).

Phase Contrast

Phase contrast arises from the interference between the undeflected wave and the waves scattered but still accepted by the objective aperture (*15*). Being an interference effect it depends on coherent wave amplitudes rather than intensities as in Eq. (1). The contrast is thus proportional to t rather than t^2 and dominates over diffraction contrast for sufficiently small particles ($t \lesssim 1.5$ nm) or when large objective apertures are used (*11*). The necessary coherence is easily destroyed by stray fields, insufficiently coherent illumination, and incoherent scattering in the substrate if it is too thick.

The simplest cause of phase contrast is the refractive index phase shift factor, $\exp(i\pi t/\xi_0)$, incurred when an electron wave passes through a crystal of thickness t

(*14*). Since for Pd, $\xi_0 \simeq 10$ nm, phase changes of a radian can occur in 3-nm-thick crystals. This phase shift would be expected to vary across a crystallite, and thus (because of defocus and spherical aberration in the objective lens) gives rise to contrast in the form of a Fresnel fringe structure (*16*). Such Fresnel fringes vary in a complex way with defocus and can interfere with the weak amplitude contrast present in small crystallites.

Figures 2a–c illustrate the variation of phase contrast with defocus. The specimen is 1 wt% Pd-on-charcoal, and particles A and B (thickness $\simeq$ 4 nm) show normal dark contrast when the objective lens is underfocused by 400 nm (Fig. 2a), but show very poor contrast when overfocused by 400 nm (Fig. 2b). With further overfocus, A and B reverse their contrast, showing up bright against the substrate (Fig. 2c). The defocus range necessary for these contrast changes to occur decreases for smaller crystallites, and it becomes questionable whether or not subnanometer-size clusters can be reliably detected against the noisy image structure of the substrate. Furthermore, as emphasized by Flynn *et al.* (*11*), height differences within a sample may introduce sufficient focus variation to affect the visibility and apparent size of otherwise similar subnanometer clusters.

A further phase contrast related effect is shown on particle C in Fig. 2b. Slight movement of the specimen has rotated C into a Bragg reflecting condition (particle C is not diffracting in Figs. 1a and c). Unlike the micrographs in Fig. 1, the objective aperture here is large enough to accept the Bragg diffracted beams (the (200) and ($\bar{2}$00)), but because of intrumental aberrations these beams do not recombine with the main beam, but instead appear as bright "ghosts" on either side of the particle (*17*). Subsequently, the particle displays strong diffraction contrast. By altering the objective lens defocus, the ghosts may be allowed to recombine with the central image. Provided the main beam and diffracted beam remain mutually coherent, they will then interfere to produce a lattice image.

Lattice images have been used to study

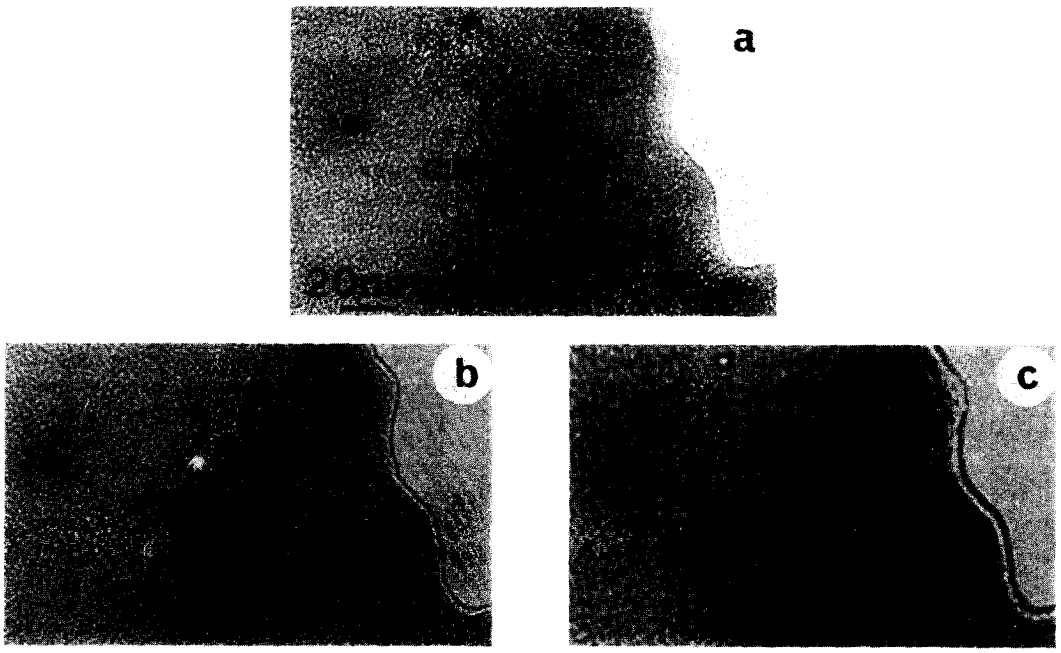

FIG. 2. Phase contrast in small Pd particles (1 wt% Pd-on-charcoal). (a) 400-nm underfocus; (b) 400-nm overfocus; (c) 800-nm overfocus.

the crystalline structure of small particles (*7, 18*). However, care must be taken not to make too naive an interpretation of such images, since the fringes do not necessarily coincide with the lattice planes and can appear to bend because of varying crystallite thickness (*14*).

Dark-Field Contrast

By tilting the illumination so that the incident beam is no longer accepted by the objective aperture, dark-field images can be generated, formed entirely by scattered electrons (*2, 7, 19*). This method has some advantages both for particle visibility and for imaging of inner structure, since the range of scattering angles selected can, for instance, be adjusted to include a particular Bragg reflection. Difficulties can arise, however, in the case of very small particles.

Figure 3a shows a tilted dark-field image of the same region as in Figs. 2a–c. Not all of the larger crystallites are detected, since they are not all diffracting into the objective aperture. However, the aperture is also collecting some scattered signal from the substrate, and this is imaged as speckle (*20*). This effect arises from the chance superposition of substrate atomic images and could easily be confused with images of small catalyst particles. The detection of such particles is consequently extremely difficult to carry out reliably with the usual bright- or dark-field methods. Some improvement can be obtained by using hollow-cone dark-field illumination as shown in Fig. 3b where the effect is to suppress the random substrate speckle by averaging it out relative to the image of the small particles (*21*). No extra particle images appear to be visible in Fig. 3b compared to Fig. 3a, but the background intensity level from the support may still be sufficient to destroy the visibility of extremely small clusters (*10*).

For the imaging of the very smallest heavy-atom clusters on disordered light-atom supports, the hollow-cone dark-field method can be extended by carrying out the imaging using the annular detector in the scanning transmission electron microscope (STEM) where the larger hollow-cone angles are available in addition to a variety of on-line image processing techniques. In the Z contrast technique, successfully used by Crewe *et al.* (*22*) for the imaging of single heavy atoms on thin amorphous carbon supports, the annular detector signal can be divided by the small-angle energy loss signal to yield greatly improved images. This technique has also been used quite successfully on catalyst specimens (*23*) to reveal small heavy-atom clusters both on amorphous carbon and on γ-alumina supports. Figure 4 shows the Z contrast technique applied to the specimen of 1 wt% Pd-on-charcoal. Figure 4a is the ratio micrograph of the annular detector signal divided by the energy loss signal and shows small Pd clusters not visible in the zero energy loss signal (Fig. 4b). In the case of crystalline supports, Bragg reflection effects in the support can still affect the visibility of clusters.

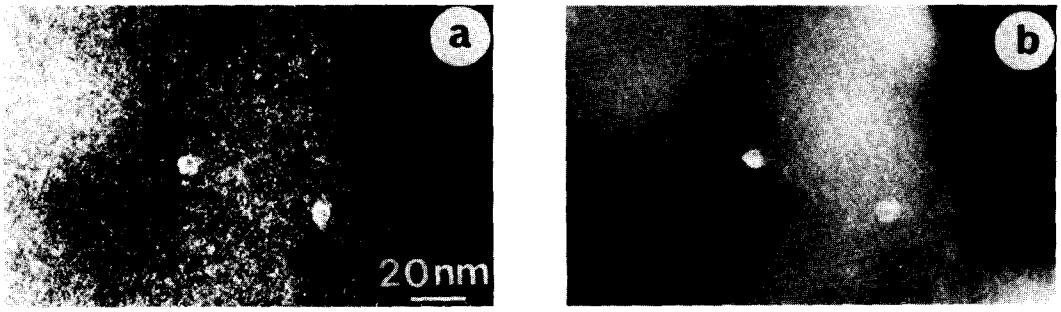

FIG. 3. (a) Tilted dark-field image; (b) hollow-cone dark-field image. Both images are of the area in Fig. 2.

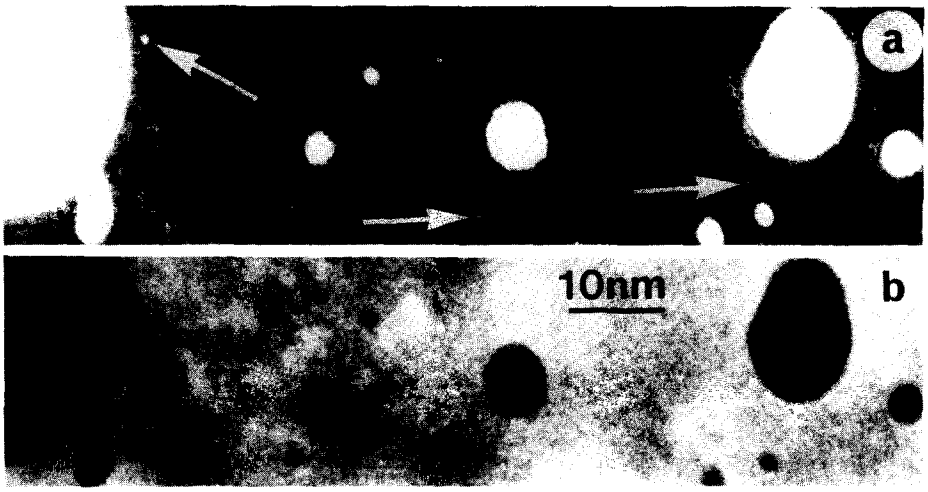

FIG. 4. (a) Ratio of the annular detector signal to the energy loss signal on the STEM, (b) STEM zero energy loss signal.

We would conclude that a great deal can probably be learned about the structure of heterogeneous catalysts using both the well-established as well as the more recent techniques of electron microscopy. Errors of interpretation can easily occur, however, if continuous attention is not paid to the scattering mechanisms of image contrast.

ACKNOWLEDGMENTS

We are grateful to Johnson Matthey Ltd. for supplying the specimens. Financial support from the Science Research Council for a CASE studentship (M.M.J.T.) is gratefully acknowledged.

REFERENCES

1. Yacamán, M. J., and Ocaña, Z. T., *Phys. Status Solidi* A42, 571 (1977).
2. Avery, N. R., and Sanders, J. V., *J. Catal.* **18**, 129 (1970).
3. Marks, L. D., and Howie, A., *Nature (London)* **282**, 196 (1979).
4. Dautzenberg, F. M., and Wolters, H. B. M., *J. Catal.* **51**, 26 (1978).
5. Nakamura, M., Yamada, M., and Amano, A., *J. Catal.* **39**, 125 (1975).
6. Prestridge, E. B., and Yates, D. J. C., *Nature (London)* **234**, 345 (1971).
7. Gillet, M., *Surface Sci.* **67**, 139 (1977).
8. Yang, C. Y., Heinemann, K., Yacamán, M. J., and Poppa, H., *Thin Solid Films* **58**, 163 (1979).
9. Pope, D., Smith, W. L., Eastlake, M. J., and Moss, R. L., *J. Catal.* **22**, 72 (1971).
10. Freeman, L. A., Howie, A., and Treacy, M. M. J., *J. Microsc.* **111**, 165 (1977).
11. Flynn, P. C., Wanke, S. E., and Turner, P. S., *J. Catal.* **33**, 233 (1974).
12. Prestridge, E. B., Via, G. H., and Sinfelt, J. H., *J. Catal.* **50**, 115 (1977).
13. Yates, D. J. C., Murrell, L. L., and Prestridge, E. B., *J. Catal.* **57**, 41 (1979).
14. Hirsch, P. B., Howie, A., Nicholson, R. B., Pashley, D. W., and Whelan, M. J., "Electron Microscopy of Thin Crystals," 2nd rev. ed. Krieger, New York, 1977.
15. Born, M., and Wolf, E., "Principles of Optics: Electromagnetic Theory of Propagation Interference and Diffraction of Light," 5th ed., p. 224. Pergamon, New York, 1975.
16. Hall, C. R., and Hines, R. L., *Phil. Mag.* **21**, 1175 (1970).
17. Heinemann, K., *Optik* **34**, 113 (1971).
18. Komoda, T., *Japan. J. Appl. Phys.* **7**, 27 (1968).
19. Granqvist, C. G., and Buhrman, R. A., *Japan, J. Appl. Phys.* **47**, 2200 (1976).
20. Howie, A., Krivanek, O. L., and Rudee, M. L., *Phil. Mag.* **27**, 235 (1973).
21. Gibson, J. M., Howie, A., and Stobbs, W. M., *Inst. Phys. Conf. Ser.* No. 36, p. 275 (1977).
22. Crewe, A. V., Langmore, J. P., and Isaacson, M. S., *in* "Physical Aspects of Electron Microscopy and Microbeam Analysis" (B. M. Siegel and D. R. Beaman, Eds.), p. 47. Wiley, New York, 1975.
23. Treacy, M. M. J., Howie, A., and Wilson, C. J., *Phil. Mag.* **A38**, 569 (1978).

M. M. J. TREACY
A. HOWIE

University of Cambridge
Madingley Road
Cambridge CB3 0HE
England

Received September 11, 1979